

ONE-ARMED SPIRAL INSTABILITY IN A
SLOWLY ROTATING, POST-BOUNCE SUPERNOVA CORECHRISTIAN D. OTT¹, SHANGLI OU², JOEL E. TOHLINE² AND ADAM BURROWS³*Submitted to ApJL; AEI-2005-021*

ABSTRACT

A three-dimensional, Newtonian hydrodynamical technique is used to follow the post-bounce phase of a stellar core collapse event. For realistic initial data we have employed post core-bounce snapshots of the iron core of a $20 M_{\odot}$ star from the study of Ott et al. (2004). The models exhibit strong differential rotation, but have centrally condensed density stratifications. We demonstrate for the first time that such post-bounce cores are subject to a so-called low- $T/|W|$ nonaxisymmetric instability and, in particular, can become dynamically unstable to an $m = 1$ - dominated spiral mode at $T/|W| \sim 0.08$. We calculate the gravitational wave emission by the instability via the quadrupole formula and find that the emitted waves may be detectable by current and future gravitational wave observatories from anywhere in the Milky Way.

Subject headings: hydrodynamics - instabilities - gravitational waves - stars: neutron - stars: rotation

1. INTRODUCTION

Rotational instabilities are potentially important in the evolution of newly-formed proto-neutron stars (proto-NSs). In particular, immediately following the pre-supernova collapse – and accompanying rapid spin up – of the iron core of a massive star, nonaxisymmetric instabilities may be effective at redistributing angular momentum within the core. By transferring angular momentum out of the centermost region of the core, nonaxisymmetric instabilities could help explain why the spin periods of newly formed pulsars are longer than what one would expect from state-of-the-art stellar evolution calculations that assume angular momentum is conserved everywhere during core collapse (Heger et al. 2000, Hirschi et al. 2004, Heger et al. 2004). Alternatively, in situations where the initial collapse “fizzles” and the proto-NS is hung up by centrifugal forces in a configuration below nuclear density, a rapid redistribution of angular momentum would facilitate the final collapse to NS densities. The time-varying mass multipole moments that would result from nonaxisymmetric instabilities in proto-NSs may also produce gravitational wave signals that are of sufficient amplitude to be detected by the burgeoning, international array of gravitational-wave interferometers. The analysis of such signals would provide us with the unprecedented ability to directly monitor the formation of NSs and, perhaps, black holes.

In this letter, we present results from numerical simulations that show the spontaneous development of a spiral-shaped instability during the post-bounce phase of the evolution of a newly formed proto-NS. These are the most realistic such simulations performed, to date, because the pre-collapse iron core has been drawn from the central region of a realistically evolved $20 M_{\odot}$ star, and the collapse of the core as well as the post-bounce phase of the evolution have been modelled in a dynamically self-consistent manner. A nonaxisymmetric instability develops in the proto-NS even though it has a relatively low ratio of rotational to gravitational potential energy, $\beta \equiv T/|W| \sim 0.08$. This is significant, but perhaps not

surprising given the recent studies by Centrella et al. (2001), Shibata et al. (2002, 2003), and Saijo et al. (2003). We examine what structural properties of the proto-NS might be responsible for the excitation of an $m = 1$ - dominated spiral mode, and examine what the consequences are of the mode’s nonlinear development.

2. NUMERICAL SIMULATION

The results presented in this letter are drawn from three-dimensional (3D) hydrodynamical simulations that follow approximately 130 ms of the “post-bounce” evolution of a newly forming proto-NS. Before presenting the details of these simulations, however, it is important to emphasize the broader evolutionary context within which they have been conducted and, specifically, from what source(s) the initial conditions for the simulations have been drawn. The two simulations presented here cover the final portion (Stage 3) of a much longer, three-part evolution that has also included: (Stage 1) the main-sequence and post-main-sequence evolution of a spherically symmetric, $20 M_{\odot}$ star through the formation of an iron core that is dynamically unstable toward collapse; and (Stage 2) the axisymmetric collapse of this unstable iron core through the evolutionary phase where it “bounces” at nuclear densities.

2.1. *Preceding Evolutionary Stages*

Stage 1 of the complete evolution was originally presented as model “S20” by Woosley & Weaver (1995). The initial configuration for this model was a chemically homogeneous, spherically symmetric, zero-age main-sequence star with solar metallicities. Evolution up to the development of an unstable iron core took some 2×10^7 yr of physical time. In Stage 2 the spherically symmetric model from Stage 1 was mapped onto the two-dimensional (2D), axisymmetric grid of the hydrodynamics code “VULCAN/2D” (Livne 1993) and evolved as model “S20A500 β 0.2” by Ott et al. (2004). Rotation was introduced into the core with a radial angular velocity profile $\Omega(\varpi) = \Omega_0[1 + (\varpi/A)^2]^{-1}$ (where ϖ is the cylindrical radius), and the ensuing axisymmetric collapse was followed. As is indicated by the suffix assigned to this model’s name in Ott et al. (2004), the scale length in the initially prescribed rotation law was set to $A = 500$ km, and $\Omega_0 = 3.36 \text{ rad s}^{-1}$ was chosen so that, initially, $\beta = 0.0020$. The axisymmetric col-

¹ Max-Planck-Institut für Gravitationsphysik, Albert-Einstein-Institut, Am Mühlenberg 1, 14476 Golm, Germany; cott@aei.mpg.de

² Department of Physics & Astronomy, Louisiana State University, Baton Rouge, LA 70803

³ Steward Observatory & the Department of Astronomy, The University of Arizona, Tucson, AZ 85721

lapse was modelled adiabatically — that is, radiation transport mechanisms were ignored — and nuclear reaction networks were eliminated, but the full Lattimer–Swesty equation of state (LSEOS; see Lattimer & Swesty 1991 and Thompson et al. 2003) was incorporated.

During Stage 2, the innermost region of the unstable iron core collapsed homologously and, in ≈ 0.5 s, approached nuclear densities. Due to angular momentum conservation, the core spun up considerably during collapse; at the time of the bounce, the rotational energy parameter had increased to $\beta_b = 0.0896$. As a result, the core bounce was aided as much by increased centrifugal forces as it was by the rapidly stiffening equation of state at nuclear densities. After bounce, the core expanded coherently, leading to an almost order-of-magnitude drop in the maximum density. This expansion was then reversed when gravitational forces again began to dominate over pressure gradients and centrifugal forces. In this way, the rapidly spinning, post-bounce core underwent several damped-harmonic-oscillator like cycles.

Ott et al. (2004) followed the axisymmetric evolution of model S20A500 β 0.2 for approximately 140 ms after the time of its initial bounce, t_b . Initial models for our fully 3D, Stage 3 simulations have been drawn from the S20A500 β 0.2 evolution, at times shortly after $t = t_b$.

2.2. Stage 3: This Investigation

In order to study the possible development of nonaxisymmetric structure in a newly forming proto-NS, we mapped the VULCAN/2D model into the fully 3D hydrodynamical code FLOW•ER (Motl et al. 2002). FLOW•ER uses an explicit finite-differencing scheme that is second-order accurate in both time and space to solve equations governing a Newtonian self-gravitating fluid system on a cylindrical coordinate mesh. In this work, we have adopted an ideal-fluid EOS to describe the fluid’s thermodynamic properties: $p = (\Gamma - 1)\epsilon\rho$, where ρ is the mass density, p is the pressure, Γ is the chosen adiabatic exponent, and ϵ is the specific internal energy. For sub-nuclear density matter — specifically, for $\rho < \rho_{\text{nuc}} \equiv 2 \times 10^{14} \text{ g cm}^{-3}$ — Γ is set to 1.325, which approximates the Γ given by the LSEOS in VULCAN/2D in the sub-nuclear density regime and the given conditions. For $\rho > \rho_{\text{nuc}}$, we have set $\Gamma = 2.0$ to mimic the effects of nuclear repulsive forces. In an attempt to minimize the inconsistencies that might arise when switching from the LSEOS of VULCAN/2D to FLOW•ER’s simple ideal-fluid EOS, we used the VULCAN/2D pressures and densities to calculate the internal energy in FLOW•ER at the time of mapping between the codes. FLOW•ER’s uniform cylindrical grid was constructed in such a way that it enclosed the innermost 140 km of model S20A500 β 0.2, containing around $1.4 M_\odot$ ($\sim 75\%$ of the mass that was on the VULCAN/2D grid at the post-bounce stage).

The Ott et al. (2004) model was mapped onto FLOW•ER’s grid at two different times during its post-bounce evolution: Model “**Q15**” was evolved on a grid with (98, 128, 194) zones in (ϖ, ϕ, Z) and mapped at $t - t_b = 15$ ms when the core was in the middle of its second post-bounce expansion phase. Upon introduction into the 3D code, its density field was perturbed with a 0.1% amplitude, bar-like $m = 2$ seed. Model “**W5**” was evolved on a higher resolution (130, 256, 194) grid, beginning at $t - t_b = 5$ ms when the model reached its first density minimum after bounce. Random perturbations of 0.02% amplitude were imposed on the densities at mapping. Both models were evolved up to a time $t - t_b \approx 130$ ms.

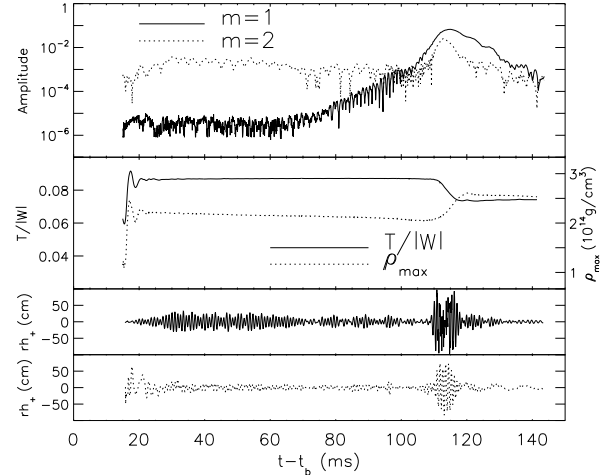


FIG. 1.— Time-evolution of various physical quantities is shown for model **Q15**; time (in ms) is given relative to t_b . Top: Globally-averaged amplitude of $m = 1$ (solid curve) and $m = 2$ (dotted curve) distortions. Middle: The rotational energy ratio β (solid curve) and the core’s maximum density ρ_{max} (dotted curve). Bottom: Product of the gravitational-wave strain h_+ and the distance to the source r as viewed down the rotation (z) axis (solid curve) and as viewed along the x -axis (dotted curve).

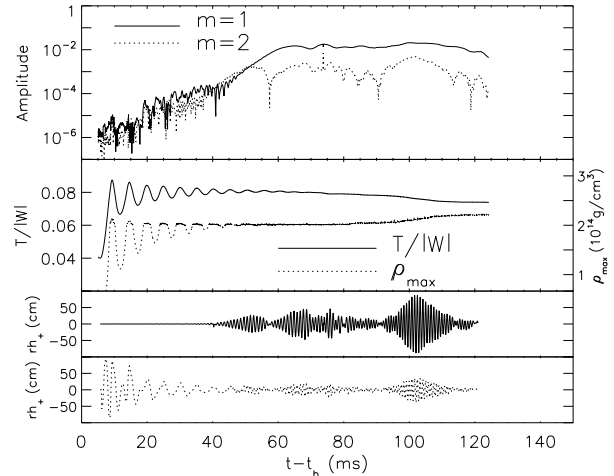


FIG. 2.— Same as Fig. 1, but for model **W5**.

3. RESULTS

The key results of our 3D evolutions are displayed in Fig. 1 (for model **Q15**) and Fig. 2 (for model **W5**). In the top panel of both figures, the time-dependent behavior of the global dipole ($m = 1$; solid curve) and quadrupole ($m = 2$; dotted curve) moments (Saijo et al. 2003) are plotted to illustrate how, and on what timescale, nonaxisymmetric structure developed. The time-dependent behavior of the rotational energy parameter, β (solid curve), and the core’s maximum density, ρ_{max} (dotted curve), are shown in the middle section of the figures. The bottom third of both figures displays the amplitude of the gravitational radiation that would be emitted from each model as estimated by the post-Newtonian quadrupole formalism (see, eg., Misner et al. 1973); specifically, for each model the time-dependent behavior of the “plus polarization” h_+ of the gravitational-wave strain is shown as seen by an observer looking down the rotation axis (solid curve) or perpendicular to that axis (dotted curve). The “cross polarization” h_\times exhibits very similar features and amplitudes to those of h_+ . Hence, we have omitted it from the plots to

save space. In order to avoid adopting one specific source distance r , in the bottom segments of Figs. 1 and 2 we have actually plotted the product rh_+ . For a core-collapse event within the Milky Way at a distance $r = 10$ kpc, an amplitude $rh_+ = 100$ cm in these figures translates into a dimensionless strain $h_+ = 3.2 \times 10^{-21}$.

Because nonaxisymmetric perturbations were initially introduced into both models at a very low amplitude ($\delta\rho/\rho \sim 10^{-3}$ in model **Q15** and $\sim 10^{-4}$ in model **W5**), the early phase of both evolutions resembled closely the post-bounce evolution reported by Ott et al. (2004). The core remained essentially axisymmetric and displayed the expected collapse/bounce/post-bounce dynamics. Here, this is illustrated best by the oscillations in $\beta(t)$ and $\rho_{\max}(t)$ that are shown in Fig. 2 for model **W5**; the characteristic (dynamical) time between successive “radial” bounces is $2\tau_{\text{dyn}} \sim 4$ ms (consistent with a mean core density $\bar{\rho} \sim (\pi G \tau_{\text{dyn}}^2)^{-1} = 1.2 \times 10^{12} \text{ g cm}^{-3}$) and the axisymmetric oscillations persist for ~ 50 ms. The curves of $h_+(t)$ for model **W5** also signal that the dynamics is essentially axisymmetric: as viewed along the x -axis, the gravitational-wave strain exhibits oscillations of diminishing amplitude, as reported in Ott et al. (2004), but for the first ~ 40 ms after t_b , essentially no gravitational-wave radiation is emitted along the z -axis. In model **Q15**, fewer “radial” bounces occur, they damp out somewhat more rapidly, and the resulting $h_+(t)$ signal is weaker as viewed along the x -axis. This is, in part, because the post-bounce core configuration was introduced into FLOW•ER at a later time ($t - t_b = 15$ ms for model **Q15** instead of $t - t_b = 5$ ms for model **W5**) and, in part, because the effects of numerical damping are inevitably more apparent when a simulation is run on a grid having lower spatial resolution. As is illustrated by the solid $h_+(t)$ curves in the bottom panels of Figs. 1 and 2, at early times the amplitude of the gravitational radiation that would be emitted along the z -axis is larger in model **Q15** than in model **W5**. This reflects the fact that the nonaxisymmetric perturbation that was initially introduced into model **Q15** was larger and it had an entirely $m = 2$ character. (Compare the amplitude of the dotted curves at early times in the top panels of Fig. 1 and Fig. 2.)

Although in model **Q15** the post-bounce core was subjected to a pure, $m = 2$ bar-mode perturbation when it was mapped onto the FLOW•ER grid, the amplitude of the model’s mass-quadrupole distortion did not grow perceptibly during the first 100 ms (~ 50 dynamical times) of the model’s evolution (Fig. 1). That is, the model appeared to be dynamically stable to the bar-mode perturbation. However, as the solid curve in the same figure panel shows, the model spontaneously developed an $m = 1$ “dipole” distortion even though the initial density perturbation did not contain any $m = 1$ contribution. As early as $t - t_b \approx 70$ ms, a globally coherent $m = 1$ mode appeared out of the noise and grew exponentially on a timescale $\tau_{\text{grow}} \approx 5$ ms. At $t - t_b \approx 100$ ms, the amplitude of this $m = 1$ distortion surpassed the amplitude of the languishing $m = 2$ structure and, shortly thereafter, it became nonlinear. At $t - t_b \approx 100$ ms, the quadrupole distortion also began to amplify, but it appears to have only been following the exponential development of the $m = 1$ mode. An analysis of the oscillation frequency of both modes reveals them to be harmonics of one another. As the top panel of Fig. 2 illustrates, the same $m = 1$ mode developed spontaneously out of the 0.02% amplitude, random perturbation that was introduced into model **W5**. The mode reached a nonlinear am-

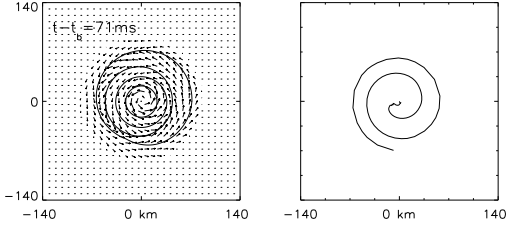


FIG. 3.— The equatorial-plane structure of model **W5** is shown at time $t - t_b = 71$ ms. Left: Two-dimensional isodensity contours with velocity vectors superposed; contour levels are (from the innermost, outward) $\rho/\rho_{\max} = 0.15, 0.01, 0.001, 0.0001$. Right: Spiral character of the $m = 1$ distortion as determined by a Fourier analysis of the density distribution; specifically, the phase angle $\phi_1(\omega)$ of the $m = 1$ Fourier mode is drawn as a function of ω .

plitude somewhat earlier in model **W5** than in model **Q15**, presumably because the initially imposed random perturbation included a finite-size contribution to an $m = 1$ distortion whereas the density perturbation introduced into model **Q15** contained no $m = 1$ component. The growth timescale of the instability is $\tau_{\text{grow}} \approx 4.8$ ms for model **W5**. Although we have described the unstable $m = 1$ mode as a “dipole” mass distortion, this is somewhat misleading because in neither model did the lopsided mass distribution produce a shift in the location of the center of mass of the system. Instead, as is illustrated in Fig. 3, the mode developed as a tightly wound, one-armed spiral, very similar to the $m = 1$ - dominated structures that have been previously reported by Centrella et al. (2001) and Saijo et al. (2003).

After the spiral pattern reached its maximum amplitude in both of our model evolutions, the maximum density began to slowly increase and β started decreasing (see the middle panels of Figs. 1 and 2). Following Saijo et al. (2003), we interpret this behavior as resulting from angular momentum redistribution that is driven by the global nonaxisymmetric spiral-like deformation and by gravitational torques associated with it. As angular momentum is transported outward, the centrifugal support of the innermost region is reduced, a larger fraction of the core’s mass is compressed to nuclear densities and, in turn, β decreases because the magnitude of the gravitational potential energy correspondingly increases. Fig. 4 supports this interpretation. The top half of the figure displays the azimuthally-averaged angular velocity profile in the equatorial plane of model **W5** at four different times, and the bottom half of the figure displays the equatorial-plane density profile at these same evolutionary times. As the proto-NS evolves, we see that the outermost layers spin faster and the innermost region becomes denser. Also, as is shown in the top panel of Fig. 4, throughout most of the model’s evolution there is a radius inside the proto-NS ($\omega_{\text{CR}} \approx 12$ km) at which the angular velocity of the fluid matches the angular eigenfrequency ($\omega_{\text{CR}} = 2.5 \times 10^3 \text{ rad s}^{-1}$) of the spiral mode. Hence, it is entirely reasonable to expect that resonances associated with this “co-rotation” region are able to effect a redistribution of angular momentum in the manner described in Contopoulos (1980) or in Watts et al. (2003). As shown in the bottom panel of Fig. 4, an off-center density maximum shows up at intermediate times, but since it is within the two innermost radial grid zones, we are not sure if it is physical or an artifact due to the boundary conditions at the axis.

Finally, we note that the nonaxisymmetric structure that developed at late times ($t - t_b \approx 100$ ms) in both of our models

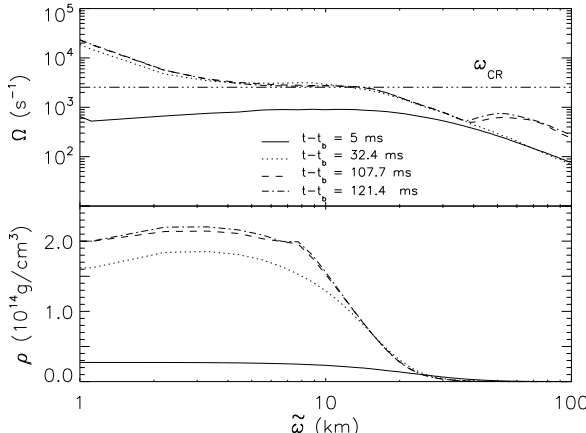


FIG. 4.—Equatorial-plane profiles of the azimuthally averaged angular velocity $\Omega(\tilde{\omega})$ (top frame) and the mass density $\rho(\tilde{\omega})$ (bottom frame) are shown at four different times during the evolution of model **W5**. Changes in these profiles at late times illustrate the effects of angular momentum redistribution due to gravitational torques exerted by the $m = 1$ spiral mode: angular momentum migrates radially outward while mass migrates radially inward. A horizontal line drawn in the top panel at $\omega_{\text{CR}} = 2.5 \times 10^3 \text{ rad s}^{-1}$ identifies the corotation radius for this one-armed spiral mode. The “kink” seen in $\rho(\tilde{\omega})$ at late times at about 8 km is connected to the discontinuous switch of the EOS Γ at ρ_{nuc} .

produced a gravitational-wave signal ($h_+(t)$, $h_\times(t)$), that was of comparable amplitude to, but had a higher frequency than, the signal that was generated by the early sequence of nearly axisymmetric “radial” core bounces (Figs. 1 & 2). Focusing on the signal that would be seen by a remote observer looking down the z -axis of model **W5** (the solid curve near the bottom of Fig. 2), however, we see that the amplitude of the gravitational-wave strain varies with time in proportion to the amplitude of the $m = 2$ mode (dotted curve in the top panel of Fig. 2) — not in proportion to the amplitude of the more dominant $m = 1$ mode, as one might naively have expected. This is because, according to general relativity, $m = 2$ (quadrupole) mass distortions are the lowest-order nonaxisymmetric time-dependent distortions that can emit gravitational waves.

4. SUMMARY AND DISCUSSION

Using the 3D, Newtonian, hydrodynamic code FLOW•ER, we have modelled the post-bounce phase of the evolution of an iron core from an evolved, $20 M_\odot$ star in order to better understand whether rotating proto-NSs are likely to be unstable toward the development of nonaxisymmetric structure. The initial conditions for our two separate simulations were drawn from an earlier study in which rotation was added to the spherical iron core at the onset of its collapse, then the “free-fall” collapse to nuclear densities was followed.

In our first simulation (model **Q15**), the rotating core was mapped from 2D onto the 3D grid at a post-bounce time of $t - t_b = 15 \text{ ms}$ and the core’s axisymmetric structure was altered slightly by the introduction of a 0.1% amplitude, bar-like density perturbation. The core was found to be dynamically stable to this pure $m = 2$ nonaxisymmetric perturbation, but it proved to be dynamically unstable toward the spontaneous development of a tightly wound, $m = 1$ spiral mode. In an effort to examine the robustness of this result, we performed a second simulation (model **W5**) in which the rotating core was mapped from 2D to 3D at an earlier time ($t - t_b = 5 \text{ ms}$), onto a grid with higher spatial resolution, and the core’s axisymmetric structure was altered by the introduc-

tion of a lower-amplitude (0.02%) and *random* density perturbation. The $m = 1$ spiral mode developed spontaneously in this model as well. Hence, we conclude that even relatively slowly rotating proto-NSs can be susceptible to the development of a spiral-shaped, $m = 1$ - dominated (dipole) mass distortion.

Even though the nonaxisymmetric distortions that developed in both of our models did not grow to particularly large nonlinear amplitudes, they produced maximum gravitational-wave amplitudes comparable to the “burst” signal produced by the preceding, axisymmetric core collapse: Model **Q15** showed the highest amplitude, $rh_{+, \text{max}} \approx 100 \text{ cm}$ at a frequency $f \approx 800 \text{ Hz}$. The peak amplitude of the axisymmetric bounce signal reported by Ott et al. (2004) was $rh_{+, \text{max}} \approx 300 \text{ cm}$ at a frequency $f \approx 400 \text{ Hz}$. If the source is located within the Milky Way, both “burst” signals may be detected by the currently operative array of gravitational wave observatories (Ott et al. 2004).

In our simulations, approximately 100 ms separated the peaks of these two gravitational-wave “bursts,” but the earlier peak near $t = t_b$ would, in practice, be unobservable if the rotation axis of the proto-NS is oriented along our line of sight, as is likely to be the case for core collapses associated with gamma-ray bursts (GRBs).

These results have demonstrated that a realistic, non-equilibrium post-bounce stellar core can become dynamically unstable to an $m = 1$ - dominated spiral instability at a value of β as low as ~ 0.08 . The value obtained in previous studies (Centrella et al. 2001, Saijo et al. 2003) for differentially rotating *equilibrium* models with a considerably simpler thermodynamic structure was $\beta \sim 0.14$. The instability appears to be related to the proto-NS’s angular velocity profile $\Omega(\tilde{\omega})$. Our post-bounce core exhibits a profile that rises toward the rotation axis in such a way that Ω exceeds the natural eigenfrequency of the spiral mode and, thereby, permits resonances to arise in association with a corotation radius inside the core.

Our simulations support the suggestion put forward by Saijo et al. (2003) that a spiral-mode instability can be effective at redistributing angular momentum within a proto-NS. In so doing, the instability can spin down the bulk of the core and, simultaneously, assist contraction of the innermost regions toward higher mean densities. As seen in our model simulations, nonaxisymmetric quadrupole mass distortions are likely to be amplified in the presence of a developing $m = 1$ mode and these time-varying structures may very well produce measurable levels of gravitational radiation if a source arises in our Galaxy.

The present study marks only one very early step in our understanding of rotational instabilities in proto-NSs. The models we have used were purely hydrodynamic, Newtonian and did not include neutrino production and transport, radiation transfer, or any of a variety of other microphysics that is likely to be relevant to these astrophysical systems. Furthermore, inconsistencies were introduced at the time of mapping between 2D and 3D when switching between the corresponding equations of state. Future, fully consistent simulations including all the relevant (micro-) physics will be needed to provide more definitive answers to these questions of stability.

Animations of the evolutions of model **Q15** and **W5** may be downloaded from <http://www.aei.mpg.de/~cott/rotinst>.

We are happy to thank L. Lindblom, I. Hawke, H. Dimmelmeier, D. Pollney, R. Walder and E. Seidel for helpful comments. This work was partially supported by National Computational Science Alliance (NCSA) under grant MCA98N043. A.B. received support from the Scientific

Discovery through Advanced Computing (SciDAC) program of the DOE, grant number DE-FC02-01ER41184. J.E.T. acknowledges support from NSF grants AST-0407070 and PHY-0326311. The numerical computations were performed on the Louisiana State University Intel Xeon cluster Superhelix, on the Peyote cluster at the Albert-Einstein-Institut and

on NCSA's Tungsten Xeon cluster. We thank the Center for Gravitational Wave Physics at Pennsylvania State University (supported by the NSF under cooperative agreement PHY01-14375) for organizing the workshop during which this collaboration was initiated.

REFERENCES

- Centrella, J., New, K., Lowe, L., & Brown, J. 2001, *ApJ Lett.*, 550, L193
 Contopoulos, G. 1980, *A&A*, 81, 198
 Heger, A., Langer, N., & Woosley, S. E. 2000, *ApJ*, 528, 368
 Heger, A., Woosley, S. E., & Spruit, H. C. 2004, submitted to *ApJ*, astro-ph/0409422
 Hirschi, R., Meynet, G., & Maeder, A. 2004, *A&A*, 425, 649
 Lattimer, J. M., & Swesty, F. D. 1991, *Nucl. Phys. A*, 535, 331
 Livne, E. 1993, *ApJ*, 412, 634
 Misner, C. W., Thorne, K. S., & Wheeler, J. A. 1973, *Gravitation* (San Francisco, U. S. A: Freeman)
 Motl, P., Tohline, J. E., & Frank, J. 2002, *ApJS*, 138, 121
 Ott, C. D., Burrows, A., Livne, E., & Walder, R. 2004, *ApJ*, 600, 834
 Saijo, M., Baumgarte, T. W., & Shapiro, S. L. 2003, *ApJ*, 595, 352
 Shibata, M., Karino, S., & Eriguchi, Y. 2002, *MNRAS*, 334, L27
 —. 2003, *MNRAS*, 343, 619
 Thompson, T. A., Burrows, A., & Pinto, P. A. 2003, *ApJ*, 592, 434
 Watts, A., Andersson, N., & Jones, D. I. 2003, astro-ph/0309554
 Woosley, S. E., & Weaver, T. A. 1995, *ApJS*, 101, 181